Available online at www.sciencedirect.com

jmr&t Journal of Materials Research and Technology

journal homepage: www.elsevier.com/locate/jmrt

Original Article

Influence of combining Al_2O_3, La_2O_3, Gd_2O_3, and Dy_2O_3 with barium borosilicate glass-ceramics: a case study of gamma radiation interaction parameters

A.M.A. Mostafa [a,***], B.O. Elbashir [b,h], Shams A.M. Issa [b,c], M.A.M. Uosif [a], Antoaneta Ene [d,1,**], Merfat Algethami [e], Omemh Bawazeer [f], E.F. El Agammy [a], Hesham M.H. Zakaly [c,g,*]

[a] Physics Department, College of Science, Jouf University, P.O. Box: 2014, Sakaka, Saudi Arabia
[b] Physics Department, Faculty of Science, University of Tabuk, Tabuk 47512, Saudi Arabia
[c] Physics Department, Faculty of Science, Al-Azhar University, Assiut, 71524, Egypt
[d] INPOLDE Research Center, Department of Chemistry, Physics and Environment, Faculty of Sciences and Environment, Dunarea de Jos University of Galati, 47 Domneasca Street, 800008 Galati, Romania
[e] Physics Department, Faculty of Science, Taif University, Taif, P. O. Box 11099, Taif 21944, Saudi Arabia
[f] Medical Physics Department, Faculty of Applied Sciences, Umm-al Qura University, Makkah, Saudi Arabia
[g] Institute of Physics and Technology, Ural Federal University, Ekaterinburg 620002, Russia
[h] Institute of Laser, Sudan University of Science and Technology, Sudan

ARTICLE INFO

Article history:
Received 15 March 2022
Accepted 13 May 2022
Available online 2 June 2022

Keywords:
Barium borosilicate glass
FLUKA Monte Carlo
Al_2O_3, La_2O_3, Gd_2O_3, and Dy_2O_3

ABSTRACT

The goal of this investigation is to test the barium boro-silicate glass-ceramics with different additives against gamma radiation using the FLUKA Monte Carlo code. On four different glass-ceramics samples, the effect of an equal quantity of Al_2O_3, La_2O_3, Gd_2O_3, and Dy_2O_3 with barium borosilicate glass-ceramics on the radiation shielding capabilities of the glass-ceramics was investigated. In the examined glass ceramics, densities were obtained to investigate glass samples. The densities obtained were 3.92, 4.432, 4.52, and 4.88 g/cm^3, respectively. BBSDy sample has the highest density which indicates that it is more effective for radiation shielding. The shielding parameters have been calculated at 0.356, 0.662, 1.173, and 1.333 MeV. The obtained results have been compared with the NistXCOM web page and Phy-X/PSD platform. The results showed a good agreement between FLUKA code, NistXCOM, and Phy-X/PSD. The calculated shielding parameters increase with additive (Al_2O_3, La_2O_3, Gd_2O_3, and Dy_2O_3). Moreover, the 50BaO−15SiO_2 −30B_2O_3−5Al_2O_3-5Dy_2O_3 specimen has the best radiation shielding features among the other glass-ceramics. In conclusion, the BBSDY sample containing 5 mol per cent 5 mol% Dy−III−Oxide would be the most effective in terms of radiation shielding, based on the

* Corresponding author. Institute of Physics and Technology, Ural Federal University, Ekaterinburg 620002, Russia.
** Corresponding author. Faculty of Sciences and Environment, Dunarea de Jos University of Galati, 47 Domneasca Street, 800008 Galati, Romania.
*** Corresponding author. Physics Department, College of Science, Jouf University, Sakaka, Saudi Arabia.
E-mail addresses: ammostafa@ju.edu.sa (A.M.A. Mostafa), Antoaneta.Ene@ugal.ro (A. Ene), h.m.zakaly@azhar.edu.eg (H.M.H. Zakaly).
[1] The work of Antoaneta Ene and the APC were supported by "Dunarea de Jos" University of Galati, Romania.
https://doi.org/10.1016/j.jmrt.2022.05.095

results obtained in this study. When Dy-III Oxide concentrations were increased, linear and mass attenuation coefficient values were significantly increased, which contributed directly to the development of radiation shielding characteristics in the glass-ceramic.

1. Introduction

A variety of ionizing radiations are now routinely used in a variety of applications, including medical imaging, radiation therapy, airport security screening, nuclear fuel imaging, structural fault diagnosis, and even space exploration, resulting in a high level of human exposure [1–4]. More than 3600 million diagnostic radiology examinations, 37 million nuclear medicine procedures, and 7.5 million radiation therapy procedures are performed worldwide each year in the medical industry. If you are exposed to scattered ionizing radiation without proper control, you are increasing your risk of developing acute radiation syndrome, which can lead to a variety of long-term health issues [5]. As a result, the use of lead (Pb) aprons by radiographers and patients alike has become commonplace when it comes to shielding against X-ray ionizing radiation [6]. However, the findings revealed that a lead apron with a thickness of 0.5 mm could block slightly more than one-third of the scattered radiation recommended to reduce frequent human exposure to radiation rather than relying on protection provided by Pb aprons to reduce frequent human exposure to radiation [7]. Pb is currently considered a less desirable material for use in wearable radiation protection due to its heavy weight (approximately 4.95 kg for a 0.50 mm Pb apron), inflexibility, poor durability, and toxicity, among other factors [8]. As a result, researchers in the field are devoting significant time and resources to the development of effective radiation protection glass materials that are free of lead.

There are modern energy **materials** called solid oxide fuel cells (SOFCs) which have several advantages that make them better than current technologies such as high electrical conversion efficiency (more than 60%), carbon capture capability, zero nitrogen dioxide emissions, fuel flexibility, low-level Noise, transport flexibility, and static applications. This technology constitutes an excellent solution for capturing visible carbon from separate fuel and airflow systems [9]. Relatively, SOFC is lower in terms of manufacturing cost and also has a higher energy density when compared to other fuel cells, but it needs sealed materials to prevent leakage. The operating temperature of this technology is in the range (of 600–1000 °C) and is dependent on the electrochemical reaction that intervenes as an influencing factor in the efficiency of cell performance, the selection of components may present a critical challenge for SOFC applications. The SOFC system's fuel efficiency and performance benefit from the high operating temperature. The high cost of the required materials, as well as the technology's long-term instability, are also disadvantages. This is why current research has focused on SOFC intermediate events in the 600 °C–800 °C working temperature range. This will reduce system costs while also enhancing long-term stability [10].

The development of appropriate sealing substances to separate fuel and air still represents a significant challenge for intermediate temperature SOFC technology. Suitable seals should be capable of withstanding temperature operations over 500 °C and tough oxidizing. These seals should also have to provide stability in long-term operation at a specific temperature. To have a hermetic seal, some crucial requirements must be prepared. It is essential that the vitreous ceramic has good adherence and adheres well to the interface. In addition, the interface must be very thin to minimize residual stresses on it. It is also necessary to maintain a minimal level of chromium diffusion at the interface between the seal and the interconnect (interconnects with chromium content such as Crofer22APU) at the seal-interconnect contact. It is necessary to prevent the diffusion of glass seal materials into the interconnect to maintain network structure [11]. Because of their low leakage rate at the SOFC operating temperature, sealants consisting of Glass and glass-ceramic are being produced and developed in large quantities. A glass sealant's viscosity status and thermal characteristics may be modified by changing the composition and crystalline volume fraction of its glass matrix to meet the criteria for sealing materials [12]. Seals must not induce deterioration of neighboring materials when exposed to high temperatures, and they must maintain long-term stability in the harsh environments that are characteristic of SOFC operating conditions. The amount to which gas fluxes within the fabric and at the interface are hindered determines the length of time the seal will last and its performance. Cracking and deterioration in the bulk of the seal, as well as gaps or separation at the interface, cause the seal's performance to fail [13].

Glass-ceramics have received a great deal of attention due to the wide range of qualities made possible by way of changing the composition of the material. It has been shown that glass-ceramics and alkaline earth metal-based silicate glasses have great promise as sealants for the purposes listed above [14]. As a candidate for sealing material, alkaline earth-based alumina silicate glasses were extensively studied. Sohn et al. have investigated the $BaO–Al_2O_3–La_2O_3–SiO_2–B_2O_3$ combination to determine its thermal and chemical stability, and their findings were published in science. According to the researchers, **The coefficients of thermal expansion** (CTE) rose with BaO percentage, and a maximum value of ~11 × 10–6 $°C^{-1}$ was obtained for 40 percent BaO and $B_2O_3/SiO_2 = 0.7$ [7]. Ley et al. studied the $SrO–Al_2O_3–La_2O_3–SiO_2–B_2O_3$ glass specimen with changing CTE in the range of (8–13) × 10^{-6} $°C^{-1}$ [15]. It was determined that the SiO_2-rich

alkaline earth metal system was the most promising of the several glass specimens tested for potential SOFC applications. Many researchers have studied the radiation shielding of various glasses [16–26]. Moreover, Other shielding materials such as concrete, alloys, polymers, and rocks have some disadvantages compared to glass materials [27–31]. The purpose of this inquiry is to report on the influence of rare earth elements such as Nd, Gd, Dy, and La on the radiation shielding properties of 50BaO-(5-x)Al_2O_3-xR_2O_3–30B_2O_3–15SiO_2 (x = 0,5) (R ≡ Nd, Gd, Dy, La) glass-ceramics.

2. Materials and methods

A total of four Barium-borosilicate-glasses-ceramics with compositions of 50BaO–15SiO_2–30B_2O_3-2 (5-x)Al_2O_3-xR_2O_3 (where R ≡ La, Gd, Dy, and x = 0, 5 mol%) have been synthesized using the melt quench technique (Table 1). The glass-ceramics samples have been coded as: (1) 50BaO–15SiO_2–30B_2O_3–5Al_2O_3–5La_2O_3 (**BBSAl**), (2) 50BaO–15SiO_2–30B_2O_3–5Al_2O_3–5La_2O_3 (**BBSLa**), (3) 50BaO–15SiO_2–30B_2O_3–5Al_2O_3-5Gd_2O_3 (**BBSGd**), and (4) 50BaO–15SiO_2–30B_2O_3–5Al_2O_3-5Dy_2O_3 (**BBSDy**) [9]. The FLUKA Mote Carlo code has been used to compute the transmission factor (TF) = [ln (I/I_0)] against glass thickness (x) for all investigated samples [32–37]. The FLUKA Monte Carlo simulation setup is shown in Fig. 1.

The obtained results have been compared with the NistX-COM web page [38] and the Phy-X/PSD platform [39]. The parameters of radiation shielding have been computed using the following equations [24,25,40–42]:

$$I = I_0 e^{-\mu x},\ \mu = \frac{\ln(I/I_0)}{x},\ \text{and}\ \mu_m = \mu\rho$$

$$T_{0.5} = \frac{\ln(2)}{\mu},\ \lambda = \frac{1}{\mu},\ \text{and}\ RPE\ (\%) = \left(1 - \ln\left(\frac{I}{I_0}\right)\right)$$

$$D_{Pb} = \left(\frac{\mu_{glass}}{\mu_{Pb}}\right)x_{glass},\ \text{and}\ H(\%) = \frac{\rho_{glass}}{\rho_{Pb}}$$

$$Z_{eff} = \frac{\sum_j f_i A_i \mu_i}{\sum_j f_j \frac{A_j}{Z_j}\mu_j}$$

where, I, I_0, μ, μ_m, $T_{0.5}$, λ, RPE, D_{Pb}, H, and Z_{eff} are the attenuated and unattenuated photon intensity, linear attenuation, and mass attenuation coefficients, half-value layer, mean free path, radiation protection efficiency, equivalent thickness of Pb, heaviness, and effective atomic number.

3. Results

For all investigated glass-ceramics at 0.356, 0.662, 1.173, and 1.333 MeV, the transmission factors (TF) against glass thickness are plotted in Fig. 2. As presented in this figure, the TF values increase with increasing photon energy for BBSAl, BBSLa, BBSGd, and BBSDy glass samples. In addition, at 0.356, 0.662, 1.173, and 1.333 MeV, TF values decreases with additive. For example, at 0.662 MeV $(TF)_{BBSAl} > (TF)_{BBSLa} > (TF)_{BBSGd} > (TF)_{BBSDy}$. This is due to the change in density (*D*) as $D_{BBSAl} < D_{BBSLa} < D_{BBSGd} < D_{BBSDy}$. Moreover, the crystalline phases formed in BBSDy are denser than those for D_{BBSAl} which leads

Table 1 – Chemical compositions and density (ρ) of studied glass-ceramics.

Code	BaO	B_2O_3	SiO_2	Al_2O_3	La_2O_3	Gd_2O_3	Dy_2O_3	ρ (g/cm^3)
BBSAl	50	30	15	5	–	–	–	3.92
BBSLa	50	30	15	–	5	–	–	4.32
BBSGd	50	30	15	–	–	5	–	4.52
BBSDy	50	30	15	–	–	–	5	4.88

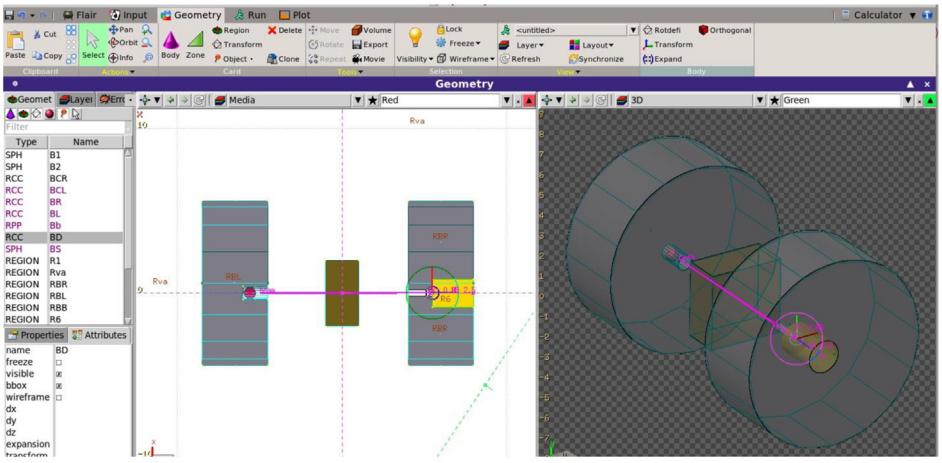

Fig. 1 – Simulation geometries of FLUKA code.

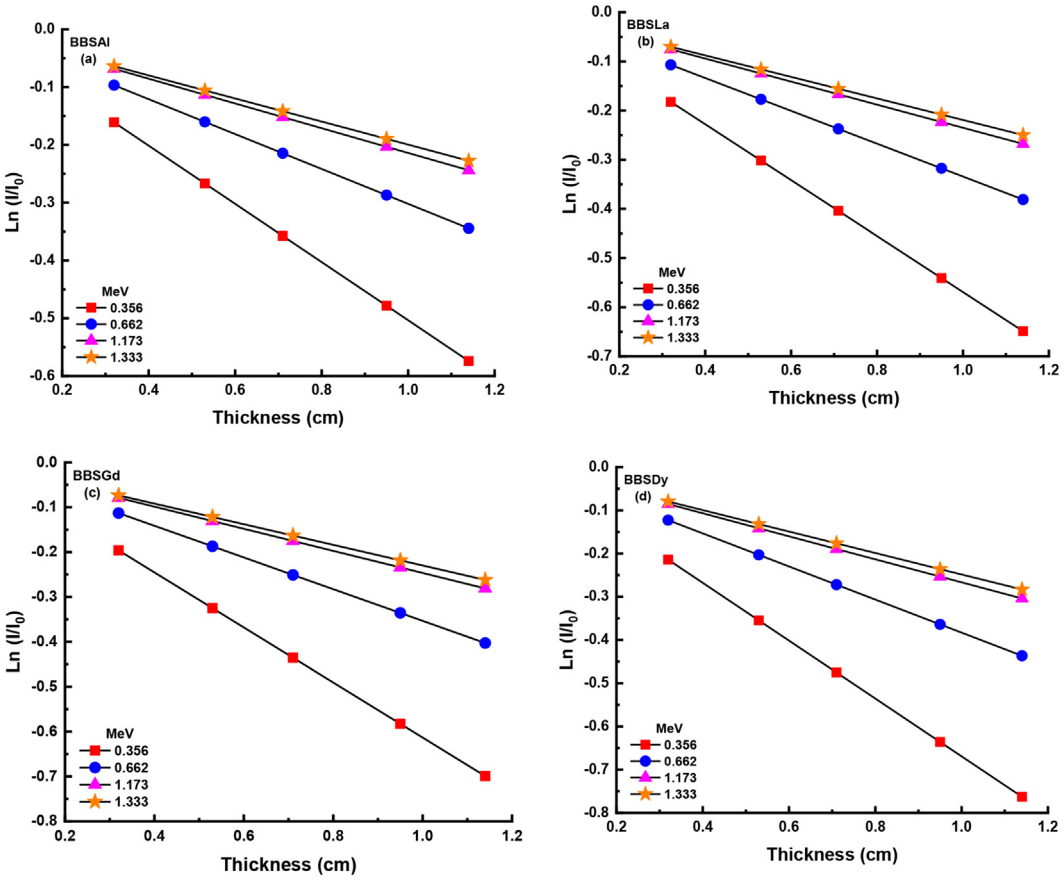

Fig. 2 – Transmission Factor (TF) against glass-ceramic thickness for all studied glass-ceramics at selected photon energy.

to compactness of the network structure. Also, it means that the photon attenuation decreases with increasing photon energy and increases with changing of additive (Al_2O_3, La_2O_3, Gd_2O_3, and Dy_2O_3). The slope of the TF-thickness graphs and glass-ceramic density has been used to measure the μ_m values for BBSAl, BBSLa, BBSGd, and BBSDy glass samples at 0.356, 0.662, 1.173, and 1.333 MeV. Gamma-rays interact with matter in three ways relying on photon energy. Photoelectric effect, Compton scattering, and pair production are the three methods in which the gamma rays interact with glasses at low, medium, and high photon energy, respectively.

Fig. 3 shows the μ_m values for all investigated glass-ceramic at selected photon energy. The μ_m values, for all glass-ceramic, decrease with increasing photon energy. At selected photon energy, the μ_m values increase with the addition of

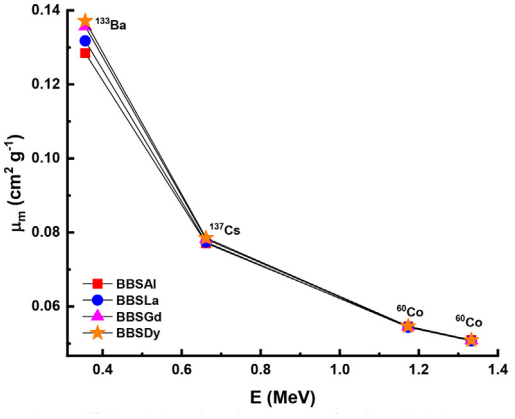

Fig. 3 – Mass attenuation coefficient (μ_m) against photon energy for all studied glass-ceramics at selected photon energy.

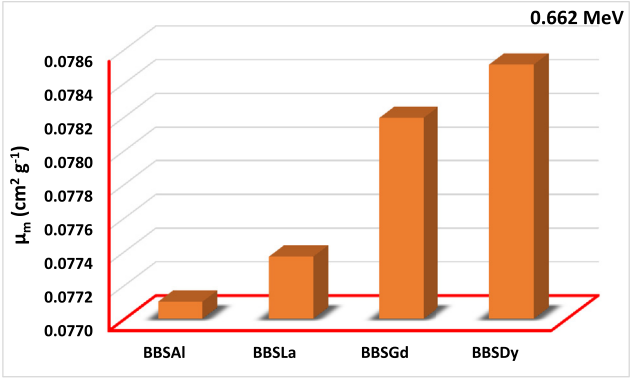

Fig. 4 – Mass attenuation coefficient (μ_m) for all studied glass-ceramics at 0.662 MeV.

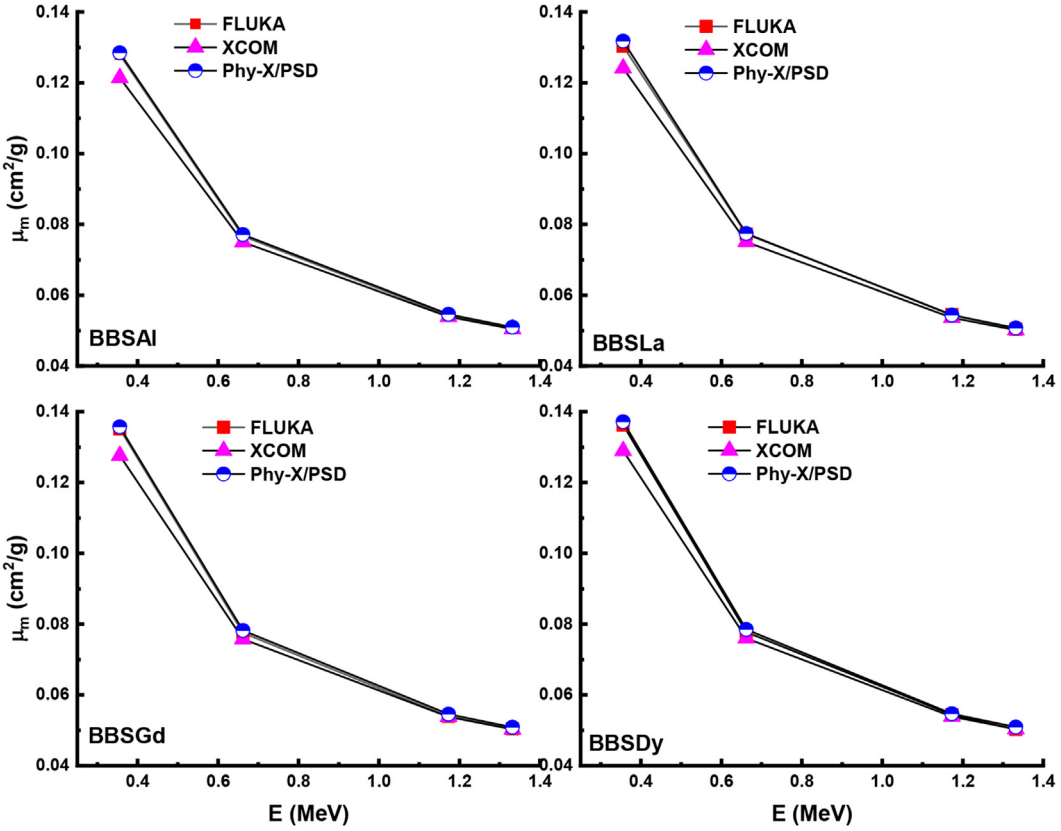

Fig. 5 – Mass attenuation coefficient (μ_m) for all studied glass-ceramics at 0.662 MeV.

Al_2O_3, La_2O_3, Gd_2O_3, and Dy_2O_3. BBSAl ($50BaO–15SiO_2–30B_2O_3–5Al_2O_3$) and BBSDy ($50BaO–15SiO_2–30B_2O_3–5Dy_2O_3$) glass-ceramic samples have the lowest and highest μ_m values, respectively. For example, at 0.662 MeV $(\mu_m)_{BBSAl} < (\mu_m)_{BBSLa} < (\mu_m)_{BBSGd} < (\mu_m)_{BBSDy}$ as present in Fig. 4. This behavior may be due to the Dy^{+3} element having the highest atomic number (66) and cationic field strength (3.64 $Å^{-2}$), compared to Gd^{+3} (3.62 $Å^{-2}$), Nd^{+3} (3.41 $Å^{-2}$), and La^{+3} (2.81 $Å^{-2}$) ions, which increases the glass density [43].

The comparison between data obtained using FLUKA Monte Carlo code, NistXCOM web page, and Phy-X/PSD platform are shown in Fig. 5. As presented in this figure, a good agreement between FLUKA Monte Carlo code, NistXCOM web page, and Phy-X/PSD platform is found. For example, at 1.173 MeV 0.0542 (FLUKA Monte Carlo code), 0.0539 (NistXCOM web page), and 0.0546 (Phy-X/PSD) (cm^2/g) are the μ_m values for BBSAl glass sample with a relative difference of 0.6% between FLUKA and NistXCOM, and 0.66% between FLUKA and Phy-X/PSD. 0.0545 (FLUKA Monte Carlo code), 0.0536 (NistXCOM web page), and 0.0544 (Phy-X/PSD) (cm^2/g) are the μ_m values for BBSLa glass sample with a relative difference of 1.59% between FLUKA and NistXCOM, and 0.21% between FLUKA and Phy-X/PSD. 0.0539 (FLUKA Monte Carlo code),

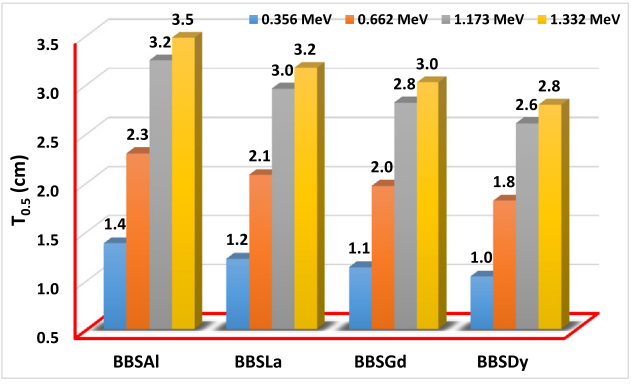

Fig. 6 – Half value layer ($T_{0.5}$) for all studied glass-ceramics at selected photon energy.

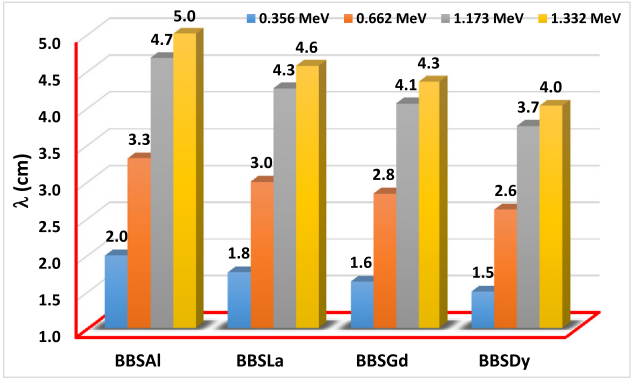

Fig. 7 – Mean free path ($T_{0.5}$) (λ) for all studied glass-ceramics at selected photon energy.

Table 2 – Linear attenuation coefficient (μ), half-value layer ($T_{0.5}$), and mean free path (λ) for all studied glass-ceramics samples.

E (MeV)	μ (cm^{-1})				$T_{0.5}$ (cm)				λ (cm)			
	BBSAl	BBSLa	BBSGd	BBSDy	BBSAl	BBSLa	BBSGd	BBSDy	BBSAl	BBSLa	BBSGd	BBSDy
0.356	0.5035	0.5692	0.6134	0.6693	1.38	1.22	1.13	1.04	1.99	1.76	1.63	1.49
0.662	0.3022	0.3342	0.3534	0.3831	2.29	2.07	1.96	1.81	3.31	2.99	2.83	2.61
1.173	0.2140	0.2349	0.2467	0.2668	3.24	2.95	2.81	2.60	4.67	4.26	4.05	3.75
1.333	0.1997	0.2191	0.2299	0.2485	3.47	3.16	3.02	2.79	5.01	4.56	4.35	4.02

0.0538 (NistXCOM web page), and 0.0546 (Phy-X/PSD) (cm^2/g) are the μ_m values for the BBSGd glass sample with a relative difference of 0.18% between FLUKA and NistXCOM, and 1.27% between FLUKA and Phy-X/PSD. 0.0544 (FLUKA Monte Carlo code), 0.0539 (NistXCOM web page), and 0.0547 (Phy-X/PSD) (cm^2/g) are the μ_m values for the BBSDy glass sample with a relative difference of 0.94% between FLUKA and NistXCOM, and −0.53% between FLUKA and Phy-X/PSD.

The half value layers ($T_{0.5}$) and the mean free path (λ) values have been calculated using μ values. $T_{0.5}$ and λ values for all investigated glass-ceramic samples at selected photon energy are plotted in Fig. 6 and Fig. 7 and the numerical values are listed in Table 2. As seen in these figures, the $T_{0.5}$ and λ values increase with increasing photon energy and decrease with additive. 1.036, 1.809, 2.598, 2.789 (cm) are the $T_{0.5}$ values for BBSDy sample at 0.356, 0.662, 1.173, and 1.333 MeV. While 1.494, 2.610, 3.749, and 4.024 (cm) are the λ values for BBSDy sample at 0.356, 0.662, 1.173, and 1.333 MeV. In addition, 1.377, 1.218, 1.130, and 1.036 (cm) are the $T_{0.5}$ values at 0.356 MeV for BBSAl, BBSLa, BBSGd, BBSDy glass samples, respectively. While 1.986, 1.757, 1.630, and 1.494 (cm) are the λ values at 0.356 MeV for BBSAl, BBSLa, BBSGd, BBSDy glass samples, respectively. The BBSDy sample, which has the highest density among otherall studied glass-ceramics, has the smallest $T_{0.5}$ values at selected photon energy when compared with other glass-ceramics (S1 [44], S2 [45], S3 [46], PCNKBi7.5 [47], Pb20 [48], PbG [49], S4 [50], S5 [51]) and different concrete (Ordinary concrete (OC), hematite-serpentine (HSC), ilmenite-limonite (ILC), basalt-magnetite (BMC), steel-scrap (SSC)) [52] (Table 3).

Table 3 – Half value layer values of BBSDy glass-ceramic sample compared to other glass-ceramics.

Glass	Half value layer ($T_{0.5}$) (cm)				Reference
	0.356 keV	0.662 keV	1.173 keV	1.333 keV	
BBSDy	1.04	1.81	2.60	2.79	This work
S1	3.46	4.48	5.87	6.27	[44]
S2	2.92	3.80	4.99	5.32	[45]
S3	2.28	3.06	4.04	4.31	[46]
PCNKBi7.5	3.02	3.92	5.14	5.49	[47]
Pb20	2.80	3.85	5.13	5.48	[48]
PbG	2.88	3.77	4.95	5.28	[49]
S4	2.28	3.06	4.04	4.31	[50]
S5	2.35	3.36	4.51	4.82	[51]
OC	2.93	3.80	4.98	5.31	[52]
HSC	2.78	3.62	4.75	5.07	[52]
ILC	2.43	3.19	4.19	4.47	[52]
BMC	2.28	2.98	3.91	4.17	[52]
SSC	1.76	2.32	3.05	3.25	[52]

The effective atomic number (Z_{eff}) and effective electron density (N_{eff}) values are plotted in Fig. 8 and listed in Table 4, respectively. Both Z_{eff} and N_{eff} values for all glass-ceramics. BBSDy sample has the highest Z_{eff} values at 0.356, 0.662, 1.173, and 1.333 MeV. While the BBSAl sample has the N_{eff} values at 1.173 and 1.333 MeV. The Radiation protection efficiency (RPE) values are shown in Fig. 9. As shown in this figure, the RPE values increase with increasing glass thickness and additive. In contrast, it decreases as the photon energy increase from 0.356 to 1.333 MeV. BBSDy sample has the largest RPE, while the BBSAl sample has the lowest. Furthermore, the lead equivalent thickness (D_{Pb}) values for BBSAl, BBSLa, BBSGd, and BBSDy glass samples at 0.32 cm and 1.14 cm have been plotted in Fig. 10 and Fig. 11, respectively. When shielding against gamma rays, the thickness of the sample required to achieve the same attenuation as Pb is known as the D_{Pd} value. For all glass-ceramics, the D_{Pd} values increase as the photon energy increase from 0.356 to 1.333 MeV. It means that at high energy, the thicker glass is requested. Also, the BBSDy

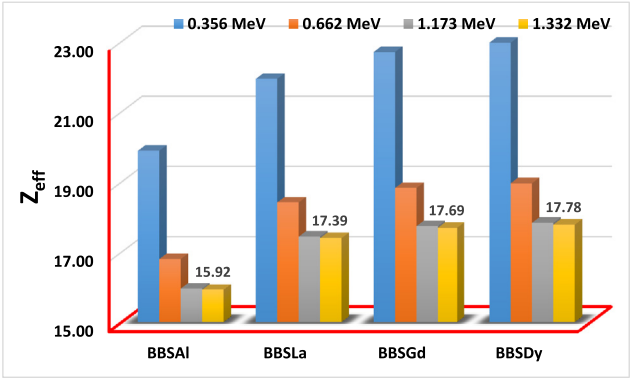

Fig. 8 – Effective atomic number (Z_{eff}) for all studied glass-ceramics at selected photon energy.

Table 4 – Effective electron density ($N_{eff} \times 10^{23}$) (electron/g) for all glass-ceramic samples.

E (MeV)	BBSAl	BBSLa	BBSGd	BBSDy
0.356	3.43	3.44	3.51	3.53
0.662	2.90	2.89	2.91	2.92
1.173	2.75	2.73	2.74	2.74
1.333	2.75	2.73	2.73	2.73

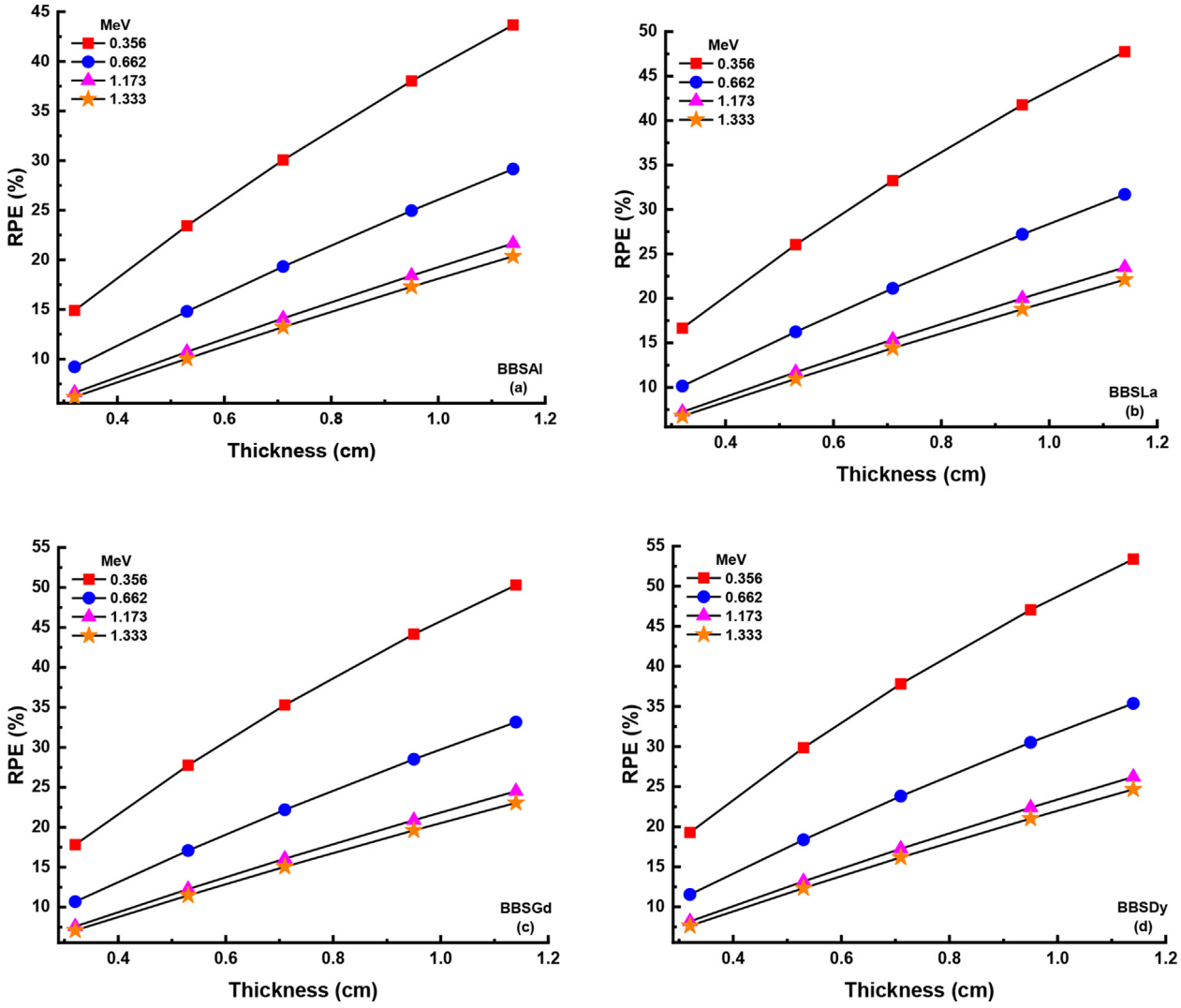

Fig. 9 – Radiation protection efficiency (RPE) for all studied glasses at selected photon energy.

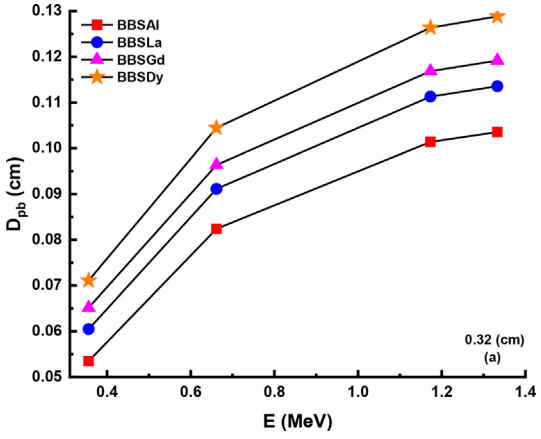

Fig. 10 – Lead equivalent thickness (D_{Pb}) for all glass-ceramics at 0.32 cm.

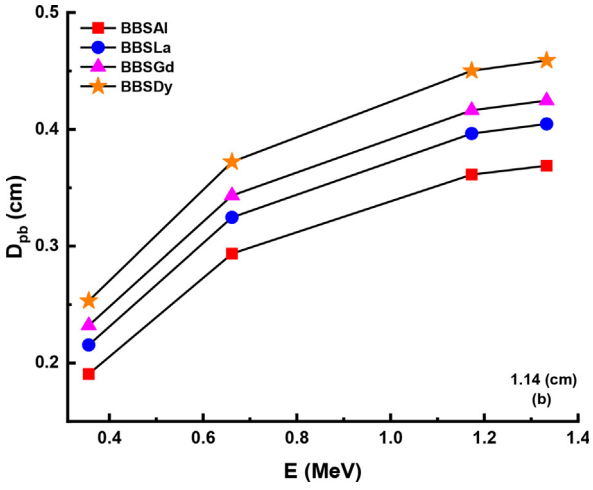

Fig. 11 – Lead equivalent thickness (D_{Pb}) for all glass-ceramics at 1.14 cm.

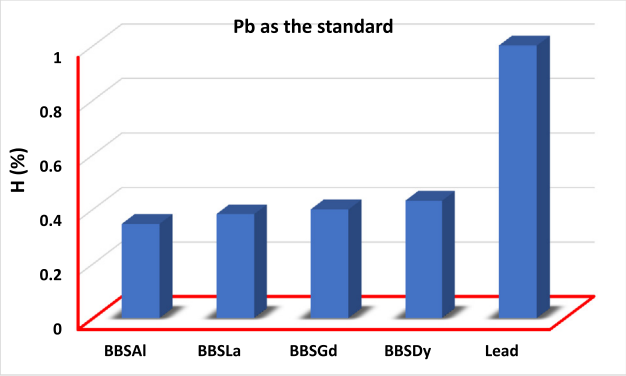

Fig. 12 – The heaviness (%) of glass-ceramics compared with lead.

glass-ceramic sample has the highest D_{Pd} value at 0.32 cm and 1.14 cm. This is due to that $D_{BBSAl} < D_{BBSLa} < D_{BBSGd} < D_{BBSDy}$. For the examined glass-ceramic with different additives, the heaviness (H%) values have been estimated using Pb as a reference. The computed H values for all studied glass-ceramic are graphed in Fig. 12. 35, 38, 40, and 43 (%) are H values for BBSAl, BBSLa, BBSGd, BBSDy glass-ceramic samples.

4. Conclusions

Specifically, the present research is focused on determining the radiological characteristics of the borosilicate glass-ceramic system, as well as the influence of adding an equal molar percentage of Al_2O_3, La_2O_3, Gd_2O_3, and Dy_2O_3 to the system on these characteristics. Four The typical melt quenching procedure was used to create glass-ceramic samples with the chemical composition $50BaO–15SiO_2–30B_2O_3–5Al_2O_3–5Al_2O_3$, $50BaO–15SiO_2–30B_2O_3–5Al_2O_3–5La_2O_3$, $50BaO–15SiO_2–30B_2O_3–5Al_2O_3\text{-}5Gd_2O_3$, and $50BaO–15SiO_2–30B_2O_3–5Al_2O_3\text{-}5Dy_2O_3$, as well as Glass. At 0.356, 0.662, 1.173, and 1.333 MeV, the shielding features of barium borosilicate glass-ceramics with different additives have been investigated. For all studied glass-ceramic samples and at selected photon energy, the mass attenuation coefficient values showed an excellent agreement with NistXCOM and Phy-X/PSD results. The glass shielding parameters such as μ_m, $T_{0.5}$, λ, RPE, D_{Pb}, H, and Z_{eff} results increase with additive. Finally, we conclude that the BBSDy glass-ceramic sample has a better attenuation feature against gamma radiation.

Author contributions

Conceptualization, M.U., and S.I.; methodology, M.U., and H.Z.; software, A.M., H.Z., E.E., O.B., and A.E.; validation, S.I., B.E., M.A., and A.E.; formal analysis, H.Z., E.E., and S.I.; investigation, A.M., O.B., M.U.; resources, E.E., and B.E.; data curation, A.M., S.I and A.E.; writing—original draft preparation, S.I., H.Z., M.A., and B.E.; writing—review and editing, A.M., M.U., and A.E.; visualization, A.M., and E.E.; supervision, H.M.H.Z., and A.E.; project administration, S.I., M.U., and B.E. All authors have read and agreed to the published version of the manuscript.

Institutional review board statement

Not applicable.

Informed consent statement

Not applicable.

Data availability statement

Data is contained within the article.

Declaration of Competing Interest

The authors declare that they have no known competing financial interests or personal relationships that could have appeared to influence the work reported in this paper.

Acknowledgments

This work was funded by the Deanship of Scientific Research at Jouf University under grant No (DSR-2021-03-03149).

REFERENCES

[1] Hoheisel M. Review of medical imaging with emphasis on X-ray detectors. Nucl Instruments Methods Phys Res Sect A Accel Spectrometers, Detect Assoc Equip 2006;563:215–24. https://doi.org/10.1016/j.nima.2006.01.123.
[2] Goitein M, Jermann M. The relative costs of proton and X-ray radiation therapy. Clin Oncol 2003;15:S37–50. https://doi.org/10.1053/clon.2002.0174.
[3] Parker HMO, Joyce MJ. The use of ionising radiation to image nuclear fuel: a review. Prog Nucl Energy 2015;85:297–318. https://doi.org/10.1016/j.pnucene.2015.06.006.
[4] Withers PJ, Preuss M. Fatigue and damage in structural materials studied by X-ray tomography. Annu Rev Mater Res 2012;42:81–103. https://doi.org/10.1146/annurev-matsci-070511-155111.
[5] Donnelly EH, Nemhauser JB, Smith JM, Kazzi ZN, Farfán EB, Chang AS, et al. Acute radiation syndrome: assessment and management. South Med J 2010;103:541–6. https://doi.org/10.1097/SMJ.0b013e3181ddd571.
[6] Hosseini SH, Askari M, Ezzati SN. X-ray attenuating nanocomposite based on polyaniline using Pb nanoparticles. Synth Met 2014;196:68–75. https://doi.org/10.1016/j.synthmet.2014.07.015.
[7] Hyun S-J, Kim K-J, Jahng T-A, Kim H-J. Efficiency of lead aprons in blocking radiation – how protective are they? Heliyon 2016;2:e00117. https://doi.org/10.1016/j.heliyon.2016.e00117.
[8] Zuguchi M, Chida K, Taura M, Inaba Y, Ebata A, Yamada S. Usefulness of non-lead aprons in radiation protection for physicians performing interventional procedures. Radiat

Protect Dosim 2008;131:531–4. https://doi.org/10.1093/rpd/ncn244.
[9] Salinigopal MS, Gopakumar N, Anjana PS, Pandey OP. Rare earth added barium alumino borosilicate glass-ceramics as sealants in solid oxide fuel cells. J Non-Cryst Solids 2022;576:121242. https://doi.org/10.1016/j.jnoncrysol.2021.121242.
[10] Ayawanna J, Kingnoi N, Laorodphan N. Effect of bismuth oxide on crystallization and sealing behavior of barium borosilicate glass sealant for SOFCs. J Non-Cryst Solids 2019;509:48–53. https://doi.org/10.1016/j.jnoncrysol.2019.01.028.
[11] Kaur G, Pandey OP, Singh K. Chemical interaction study between lanthanum based different alkaline earth glass sealants with Crofer 22 APU for solid oxide fuel cell applications. Int J Hydrogen Energy 2012;37:3883–9. https://doi.org/10.1016/j.ijhydene.2011.04.104.
[12] Dai Z, Pu J, Yan D, Chi B, Jian L. Thermal cycle stability of Al2O3-based compressive seals for planar intermediate temperature solid oxide fuel cells. Int J Hydrogen Energy 2011;36:3131–7. https://doi.org/10.1016/j.ijhydene.2010.10.086.
[13] Dev B, Walter ME, Arkenberg GB, Swartz SL. Mechanical and thermal characterization of a ceramic/glass composite seal for solid oxide fuel cells. J Power Sources 2014;245:958–66. https://doi.org/10.1016/j.jpowsour.2013.07.054.
[14] Tiwari B, Dixit A, Kothiyal GP. Study of glasses/glass-ceramics in the SrO–ZnO–SiO2 system as high temperature sealant for SOFC applications. Int J Hydrogen Energy 2011;36:15002–8. https://doi.org/10.1016/j.ijhydene.2011.04.018.
[15] Ley KL, Krumpelt M, Kumar R, Meiser JH, Bloom I. Glass-ceramic sealants for solid oxide fuel cells: Part I. Physical properties. J Mater Res 1996;11:1489–93. https://doi.org/10.1557/JMR.1996.0185.
[16] Edukondalu A, Stalin S, Reddy MS, Eke C, Alrowaili ZA, Al-Buriahi MS. Synthesis, thermal, optical, mechanical and radiation-attenuation characteristics of borate glass system modified by Bi2O3/MgO. Appl Phys A 2022;128:331. https://doi.org/10.1007/s00339-022-05475-3.
[17] Al-Buriahi MS, Sriwunkum C, Arslan H, Tonguc BT, Bourham MA. Investigation of barium borate glasses for radiation shielding applications. Appl Phys A 2020;126:68. https://doi.org/10.1007/s00339-019-3254-9.
[18] Al-Buriahi MS, Olarinoye IO, Alshahrani B, Al-Baradi AM, Mutuwong C, Arslan H. Optical and gamma-ray absorption features of newly developed P2O5–Ce2O3–La2O3 glass system. Appl Phys A 2021;127:873. https://doi.org/10.1007/s00339-021-05034-2.
[19] Al-Buriahi MS, Bakhsh EM, Tonguc B, Khan SB. Mechanical and radiation shielding properties of tellurite glasses doped with ZnO and NiO. Ceram Int 2020;46:19078–83. https://doi.org/10.1016/j.ceramint.2020.04.240.
[20] Alzahrani JS, Alrowaili ZA, Eke C, Mahmoud ZMM, Mutuwong C, Al-Buriahi MS. Nuclear shielding properties of Ni-, Fe-, Pb-, and W-based alloys. Radiat Phys Chem 2022;195:110090. https://doi.org/10.1016/j.radphyschem.2022.110090.
[21] Al-Buriahi MS, Singh VP, Alalawi A, Sriwunkum C, Tonguc BT. Mechanical features and radiation shielding properties of TeO2–Ag2O-WO3 glasses. Ceram Int 2020;46:15464–72. https://doi.org/10.1016/j.ceramint.2020.03.091.
[22] Al-Buriahi M, Alrowaili ZA, Alomairy S, Olarinoye IO, Mutuwong C. Optical properties and radiation shielding competence of Bi/Te-BGe glass system containing B2O3 and GeO2. Optik 2022;257:168883. https://doi.org/10.1016/j.ijleo.2022.168883.
[23] Alzahrani JS, Alothman MA, Eke C, Al-Ghamdi H, Aloraini DA, Al-Buriahi MS. Simulating the radiation shielding properties of TeO2–Na2O–TiO glass system using PHITS Monte Carlo code. Comput Mater Sci 2021;196:110566. https://doi.org/10.1016/j.commatsci.2021.110566.
[24] Elazaka AI, Zakaly HMH, Issa SAM, Rashad M, Tekin HO, Saudi HA, et al. New approach to removal of hazardous Bypass Cement Dust (BCD) from the environment: 20Na2O-20BaCl2-(60-x)B2O3-(x)BCD glass system and Optical, mechanical, structural and nuclear radiation shielding competences. J Hazard Mater 2021;403:123738. https://doi.org/10.1016/j.jhazmat.2020.123738.
[25] Issa SAM, Darwish AAA, El-Nahass MM. The evolution of gamma-rays sensing properties of pure and doped phthalocyanine. Prog Nucl Energy 2017;100:276–82. https://doi.org/10.1016/j.pnucene.2017.06.016.
[26] Alshahrani B, Alrowaili ZA, J. Alsufyani S, Olarinoye IO, Mutuwong C, Al-Buriahi MS. Determining the optical properties and simulating the radiation shielding parameters of Dy3+ doped lithium yttrium borate glasses. Optik 2022;250:168318. https://doi.org/10.1016/j.ijleo.2021.168318.
[27] Alshahrani B, Olarinoye IO, Mutuwong C, Sriwunkum C, Yakout HA, Tekin HO, et al. Amorphous alloys with high Fe content for radiation shielding applications. Radiat Phys Chem 2021;183:109386. https://doi.org/10.1016/j.radphyschem.2021.109386.
[28] Saeed A, Alomairy S, Sriwunkum C, Al-Buriahi MS. Neutron and charged particle attenuation properties of volcanic rocks. Radiat Phys Chem 2021;184:109454. https://doi.org/10.1016/j.radphyschem.2021.109454.
[29] Al-Buriahi MS, Alomairy S, Mutuwong C. Effects of MgO addition on the radiation attenuation properties of 45S5 bioglass system at the energies of medical interest: an in silico study. J Australas Ceram Soc 2021;57:1107–15. https://doi.org/10.1007/s41779-021-00605-1.
[30] Al-Buriahi MS, Eke C, Alomairy S, Yildirim A, Alsaeedy HI, Sriwunkum C. Radiation attenuation properties of some commercial polymers for advanced shielding applications at low energies. Polym Adv Technol 2021;32:2386–96. https://doi.org/10.1002/pat.5267.
[31] Al-Buriahi MS, Singh VP. Comparison of shielding properties of various marble concretes using GEANT4 simulation and experimental data. J Australas Ceram Soc 2020;56:1127–33. https://doi.org/10.1007/s41779-020-00457-1.
[32] Ballarini F, Battistoni G, Brugger M, Campanella M, Carboni M, Cerutti F, et al. The physics of the FLUKA code: recent developments. Adv Space Res 2007;40:1339–49. https://doi.org/10.1016/j.asr.2007.05.031.
[33] Battistoni G, Boehlen T, Cerutti F, Chin PW, Esposito LS, Fassò A, et al. Overview of the FLUKA code. Ann Nucl Energy 2015;82:10–8. https://doi.org/10.1016/j.anucene.2014.11.007.
[34] Zakaly HM, Abouhaswa AS, Issa SAM, Mostafa MYA, Pyshkina M, El-Mallawany R. Optical and nuclear radiation shielding properties of zinc borate glasses doped with lanthanum oxide. J Non-Cryst Solids 2020;543:120151. https://doi.org/10.1016/j.jnoncrysol.2020.120151.
[35] Zakaly HMH, Saudi HA, Issa SAM, Rashad M, Elazaka AI, Tekin HO, et al. Alteration of optical, structural, mechanical durability and nuclear radiation attenuation properties of barium borosilicate glasses through BaO reinforcement: experimental and numerical analyses. Ceram Int 2021;47:5587–96. https://doi.org/10.1016/j.ceramint.2020.10.143.
[36] Rashad M, Tekin HO, Zakaly HM, Pyshkina M, Issa SAM, Susoy G. Physical and nuclear shielding properties of newly synthesized magnesium oxide and zinc oxide nanoparticles.

Nucl Eng Technol 2020;52:2078–84. https://doi.org/10.1016/j.net.2020.02.013.
[37] Sallam OI, Zakaly HMH, Issa SAM, Rashad M. Fabrications a new family of samarium lead phosphate glasses, determination electrical, structural and optical properties under effect of different gamma doses. Optik 2022;249:168266. https://doi.org/10.1016/j.ijleo.2021.168266.
[38] Berger MJ, Hubbell JH, Seltzer SM, Chang J, Coursey JS, Sukumar R, et al. Photon cross sections database. 1998.
[39] Şakar E, Özpolat ÖF, Alım B, Sayyed MI, Kurudirek M. Phy-X/PSD: development of a user friendly online software for calculation of parameters relevant to radiation shielding and dosimetry. Radiat Phys Chem 2020;166:108496. https://doi.org/10.1016/j.radphyschem.2019.108496.
[40] Alatawi A, Alsharari AM, Issa SAM, Rashad M, Darwish AAA, Saddeek YB, et al. Improvement of mechanical properties and radiation shielding performance of AlBiBO3 glasses using yttria: an experimental investigation. Ceram Int 2020;46:3534–42. https://doi.org/10.1016/j.ceramint.2019.10.069.
[41] Issa SA, Zakaly HMH, Pyshkina M, Mostafa MYA, Rashad M, Soliman TS. Structure, optical, and radiation shielding properties of PVA–BaTiO3 nanocomposite films: an experimental investigation. Radiat Phys Chem 2021;180:109281. https://doi.org/10.1016/j.radphyschem.2020.109281.
[42] Issa SAM, Ali AM, Tekin HO, Saddeek YB, Al-Hajry A, Algarni H, et al. Enhancement of nuclear radiation shielding and mechanical properties of YBiBO3 glasses using La2O3. Nucl Eng Technol 2019;52:1297–303. https://doi.org/10.1016/j.net.2019.11.017.
[43] Luo Y-R. Handbook of bond dissociation energies in organic compounds. CRC Press; 2002. https://doi.org/10.1201/9781420039863.
[44] Aktas B, Yalcin S, Dogru K, Uzunoglu Z, Yilmaz D. Structural and radiation shielding properties of chromium oxide doped borosilicate glass. Radiat Phys Chem 2019;156:144–9. https://doi.org/10.1016/j.radphyschem.2018.11.012.
[45] Yalcin S, Aktas B, Yilmaz D. Radiation shielding properties of Cerium oxide and Erbium oxide doped obsidian glass. Radiat Phys Chem 2019;160:83–8. https://doi.org/10.1016/j.radphyschem.2019.03.024.
[46] Mhareb MHA, Alajerami YSM, Sayyed MI, Dwaikat N, Alqahtani M, Alshahri F, et al. Radiation shielding, structural, physical, and optical properties for a series of borosilicate glass. J Non-Cryst Solids 2020;550:120360. https://doi.org/10.1016/j.jnoncrysol.2020.120360.
[47] Al-Yousef HA, Sayyed MI, Alotiby M, Kumar A, Alghamdi YS, Alotaibi BM, et al. Evaluation of optical, and radiation shielding features of New phosphate-based glass system. Optik 2021;242:167220. https://doi.org/10.1016/j.ijleo.2021.167220.
[48] Almuqrin AH, Kumar A, Jecong JFM, Al-Harbi N, Hannachi E, Sayyed MI. Li2O-K2O-B2O3-PbO glass system: optical and gamma-ray shielding investigations. Optik 2021;247:167792. https://doi.org/10.1016/j.ijleo.2021.167792.
[49] Al-Harbi FF, Prabhu NS, Sayyed MI, Almuqrin AH, Kumar A, Kamath SD. Evaluation of structural and gamma ray shielding competence of Li2O-K2O-B2O3-HMO (HMO = SrO/TeO2/PbO/Bi2O3) glass system. Optik 2021;248:168074. https://doi.org/10.1016/j.ijleo.2021.168074.
[50] Mhareb MHA, Alqahtani M, Alajerami YSM, Alshahri F, Sayyed MI, Mahmoud KA, et al. Ionizing radiation shielding features for titanium borosilicate glass modified with different concentrations of barium oxide. Mater Chem Phys 2021;272:125047. https://doi.org/10.1016/j.matchemphys.2021.125047.
[51] Singh S, Kaur R, Rani S, Sidhu BS. Physical, structural and nuclear radiation shielding behaviour of xBaO-(0.30-x)MgO-0.10Na2O-0.10Al2O3-0.50B2O3 glass matrix. Mater Chem Phys 2022;276:125415. https://doi.org/10.1016/j.matchemphys.2021.125415.
[52] Bashter II. Calculation of radiation attenuation coefficients for shielding concretes. Ann Nucl Energy 1997;24:1389–401. https://doi.org/10.1016/S0306-4549(97)00003-0.